Integrated Sensing Arrays Based on Organic Electrochemical Transistors

JINJIE WEN (ID), **JIE XU, WEI HUANG** (ID)**, CONG CHEN** (ID)**, LIBING BAI** (ID)**, AND YUHUA CHENG** (ID)

School of Automation Engineering, University of Electronic Science and Technology of China, Chengdu 611731, China

CORRESPONDING AUTHORS: WEI HUANG; YUHUA CHENG (e-mail: whuang@uestc.edu.cn; yhcheng@uestc.edu.cn)
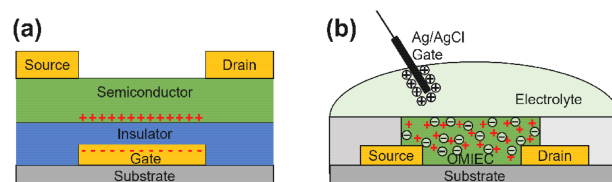
ABSTRACT Organic electrochemical transistors (OECTs), as one of the most promising sensing techniques, have shown various advantages compared to traditional means, which include ultra-high sensitivity, low driving voltage, and excellent biocompatibility for different bioelectrical and biochemical sensing. Moreover, to fully unleash the potential of OECT sensors, integrated sensing systems, especially OECT-based sensing arrays, are widely investigated due to spatiotemporal resolution, mechanical flexibility, high optical transparency, low power dissipation, and ease of fabrication. These advantages are attributed to the unique working mechanism of OECT, novel mixed ionic-electronic (semi)conductors, adaptable device geometry/structure, etc. In this review, advances in OECT-based sensing systems are systematically summarized, with a focus on the OECT-based sensing array. Furthermore, perspectives, concerning stability, cut-off frequency, integrating density, and power dissipation, are discussed based on recent studies on OECTs and their relevant sensor arrays. Last, a summary and an outlook of this field are provided.

INDEX TERMS Biosensors, organic electrochemical transistors, physiological sensing, sensing arrays.

I. INTRODUCTION

Since J. E. Lilienfeld first introduced the transistor concept in 1928, various transistors have been developed and are now the core of any electronics [1]. Among all kinds of transistors, organic electrochemical transistors (OECTs), which is developed by M. Wrighton in 1984, show extraordinary advantages for biosensing, due to their low driving voltage, high transconductance (g_m), mechanical flexibility, and biocompatibility [2], [3]. Compared with traditional transistors (for instance, thin-film transistors, TFTs) where its channel is limited at the interface of semiconductor/dielectric, modulation of the channel conductivity of OECTs relies on the ionic doping/dedoping process of the channel bulk, while high capacitance electrolyte acts as dielectric (*vide infra*) [4].

Specifically, conductivity switching of TFTs depends on the field effect induced by gate voltage (V_G). For instance, in a p-type TFT, by applying a negative V_G greater than the threshold voltage (V_{TH}) to the gate electrode, hole carriers will be accumulated at the dielectric/semiconductor interface at the semiconductor side and form a conducting channel that is typically a few nanometers thick (Fig. 1(a)) [5].


FIGURE 1. Schematic illustrations of transistor structures of a) thin-film transistor (TFT), and b) organic electrochemical transistor (OECT).

Consequently, an electrical current can flow between the source and drain electrode when a drain voltage (V_D) is applied. Thus, in typical TFTs, g_m can be expressed as:

$$g_m = (W/L)\,\mu C_{ox}\,|V_G - V_{TH}| \qquad (1)$$

where W and L are the width and length of the semiconducting channel, respectively, μ is the charge carrier mobility, and C_{ox} is the capacitance per area of the gate dielectric.

On the other hand, during the operation of a p-type OECT, when V_G is applied through an electrolyte, ions from the electrolyte will be injected into the organic (semi)conductor
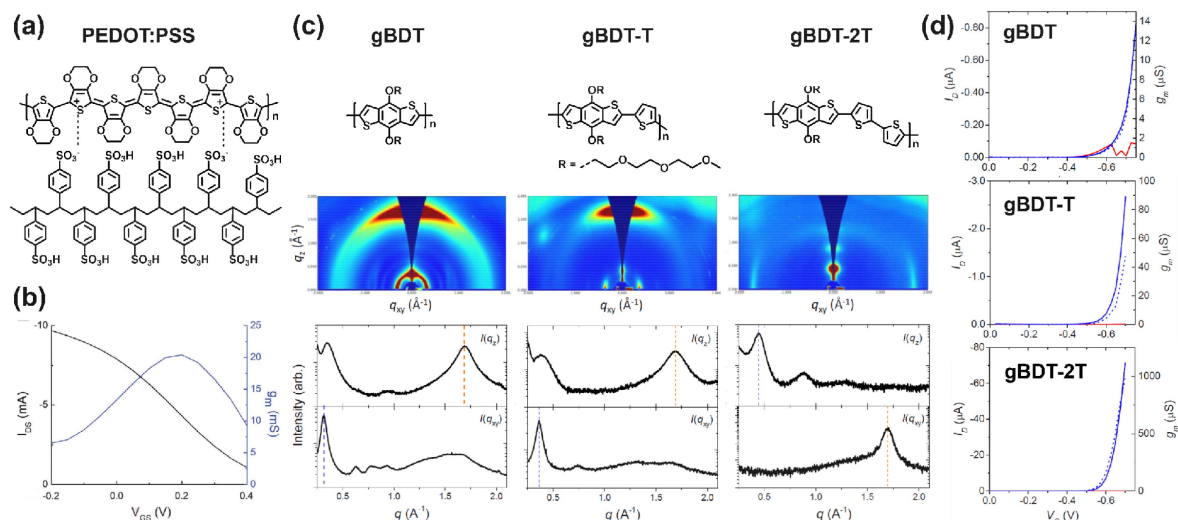
FIGURE 2. (a) Chemical structure of PEDOT: PSS along with (b) a typical transfer characteristic of a PEDOT: PSS based OECT [16]. Reproduced with permission, Copyright 2022, Wiley-VCH. (c) Chemical structures of the gBDT-based polymers, along with their corresponding grazing-incidence wide-angle Scattering (GIWAXS) plots and (d) representative transfer characteristics [15]. Reproduced with permission, Copyright 2016, American Chemical Society.

channel film, leading to changes in the doping state throughout the channel bulk (Fig. 1(b)) [6]. Thus, the conductivity of the OECT is modulated. Organic channel materials in OECTs hold the capability to conduct both ions and electrons/holes and are typically called organic mixed ionic-electronic (semi)conductors (OMIECs) [7]. Consequently, the g_m of OECTs depends on the volumetric capacitance (C^*, capacitance per unit volume), the geometry of the channel, and the mobility of the OMIEC [8]:

$$g_m = (Wd/L)\mu C^* |V_G - V_{TH}| \qquad (2)$$

where d is the thickness of the OECT channel. Note, Eq. (2) is for g_m in the saturation region. Thus, compared with typical transistors, where only planar capacitance is formed, the C^* of OECTs can be much larger due to the 3-dimensional channel geometry. Therefore, g_m in OECTs can be more than 10 mS under low driving voltage (typically lower than ± 1 V), which enables tremendous amplification capability with low power dissipation [9]. Note, in Fig. 1(b), an Ag/AgCl nonpolarizable electrode is applied to ensure all the voltage drop from V_G is located between electrolyte and OMIEC, which would lead to enhanced C^*.

As indicated above, the development of OECTs relies extensively on OMIECs. For more than a decade, research on OECTs is mostly based on poly(34-ethylene dioxythiophene) doped with poly (styrene sulfonate) (PEDOT: PSS) (Fig. 2(a)). This is due to that in the early development stage of OECTs, PEDOT: PSS is one of the rare materials that holds both decent ionic and electronic conductivity simultaneously, where the electronic conductivity can be modulated by the ionic doping level [10]. Most importantly, PEDOT: PSS is widely commercially available, which facilitated its utilization in different aspects. While for OECTs, PEDOT: PSS can be insoluble in water after being crosslinked and shows relatively good electrochemical stability in aqueous electrolytes

[11], [12], [13]. Consequently, research on OECTs based on PEDOT: PSS with high performance ($g_m > 1$ mS) and low operating voltage (< 1 V) has been extensively reported, and facilitated the development of OECTs with novel new structures and the synthesis of other OMIECs [6]. However, obvious disadvantages still exist in PEDOT: PSS based OECTs, including a small current on/off ratio (typically in the range of less than 10^3), depleting working mode (Fig. 2(b)), and inferior cycling stability compared to mature transistor techniques.

In recent years, various new OMIECs (mostly polymers, including both p- and n-type materials) for OECTs have been developed with enhanced properties [14]. Diverse polymer backbones and side chains have been adopted to maintain charge carrier mobility and ion diffusion efficiency, which are the two key aspects of high-performance OECT materials. Specifically, differences in the structures of the polymeric backbone can modulate the energy levels, polymer conformation, and interchain interactions, and thereby change the material performance, especially the carrier concentration and mobility. For instance, with the increment of the unsubstituted thiophene content in the backbone of a triethylene glycol grafted benzo[12-b:45-b']-dithiophene (gBDT) based polymer, better charge transport, and higher hole mobility can be achieved due to the polymer chain transformation from a face-on orientation to an edge-on orientation (Fig. 2(c)) [15]. By applying these materials as the OECT channel, the edge-on-oriented polymer gBDT-2T favors in-plane charge transport, leading to a drain current (I_D) of about 70 μA under a small V_G of -0.7 V. While OECTs based on gBDT and gBDT-T show much smaller I_Ds of ~0.8 μA and ~2.5 μA, respectively, under the same bias condition (Fig. 2(d)) [15].

Studies on semiconductors for organic field-effect transistors have revealed that side chains will affect molecular packing, film morphology, solubility, and consequently
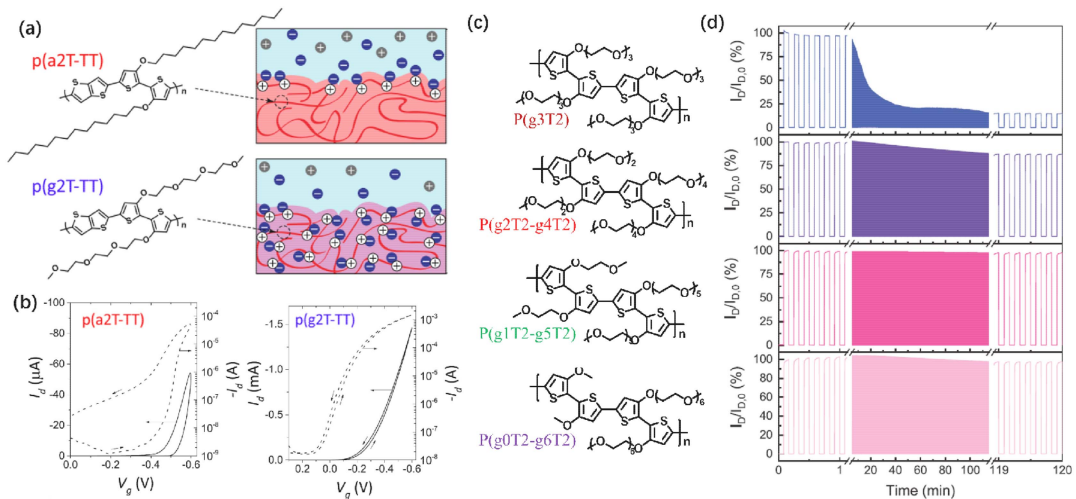
FIGURE 3. (a) Chemical structures and schematic of interactions of ions with p(a2T-TT) and p(g2T-TT). (b) Transfer characteristics of OECTs based on p(a2T-TT) and p(g2T-TT). Note, $V_D = -0.6$ V [21]. Reproduced with permission, Copyright 2016, National Academy of Sciences. (c) Chemical structures of the polymers with different EG side change lengths, along with their cycling stabilities over 2 h continuous switching [22]. Reproduced with permission, Copyright 2020, Wiley-VCH.

device performance [17], [18], [19]. While for channel materials in OECTs, side chains play an extra role, which is facilitating ion diffusion and thus affecting the doping/dedoping process. It is well known that replacing alkyl side chains with ethylene glycol (EG) chains can effectively enhance ion infiltration and transport [20]. Therefore, poly(2-(3,3'-bis(2-(2-(2-methoxy ethoxy)ethoxy)ethoxy)-[2,2'-bithiophen]-5-yl)thieno[32-b]thiophene) p(g2T-TT) with EG chains exhibits complete and reversible electrochemical doping/dedoping with high volumetric capacitance (240 F/cm^3), while with the same backbone but without EG side chains, poly(2-(3,3'-bis(tetradecyloxy)-[2,2'-bithiophen]-5-yl)thieno[32-b]thiophene) p(a2T-TT) with alkoxy side chains shows much lower effective capacitance ($\sim$10–20 μF/cm^2) (Fig. 3). Consequently, OECT based on p(g2T-TT) show much higher g_m and faster transient response, when compared to these in p(a2T-TT) based OECT (Fig. 3(b)). This result demonstrates that the EG side chains facilitate hydration and ion penetration, which is vital for high-performance OECT materials [21]. Moreover, side chain redistribution can also improve electrochemical stability. For instance, by modifying the side chain length, Moser et al. synthesized p(g3T2), p(g2T2-g4T2), p(g1T2-g5T2), and p(g0T2-g6T2) (Fig. 3(c)), where controllable swelling properties (249%, 168%, 10%, and 4% of volume increases, respectively) and enhanced cycling stability are obtained (Fig. 3(d)) [22].

Due to the developments of novel OMIECs, the performance of OECTs has been improved comprehensively and has been applied for diverse physiological sensing and human-machine/brain-computer interfaces [23], [24], [25], [26]. A typical example of stereo electroencephalography and electrocorticography (ECoG) acquired by OECTs was 30 years after the invention of such technique, where brain activity, including bicuculline-induced epileptiform spike, was

recorded successfully [14], [27]. Since then, applications utilizing OECTs in bioelectronics started to bloom. For physiological sensing, OECTs have been used for electrocardiography (ECG) [28], electromyography (EMG) [24], electroencephalography (EEG) [8], and ECoG recording [29], which cover the health monitoring and even disease diagnose of heart, eye, brain, muscular and cerebral cortex (Fig. 4(a)).

Moreover, OECTs have also been extensively studied in the biochemical sensing field (Fig. 4(b)). For example, as one of the richest sources for biochemical sensing [30], sweat, especially the ion species and concentrations in it, can provide various information about the health status of an individual/patient [31], [32]. Keene et al. integrated different ion-selective membranes with PEDOT: PSS based OECTs for NH_4^+ and Ca^{2+} sensing in sweat during physical exercise, where high ions sensitivity and selectivity were realized based on the wearable OECT patch (Fig. 4(b)i) [26]. Guo et al. reported an OECT sensor for COVID-19 antigen by utilizing gate electrodes functionalized with high-density and orientation-controlled bioconjugation of nanobody–SpyCatcher fusion proteins [33]. Such an OECT sensor has high specificity and single-molecule sensitivity, which is capable of sensing specific antigens in complex bodily fluids, e.g., saliva and serum. It is worth noting that OECT-based sensors are feasible to monitor the concentration of all physiologically relevant cations in a single system as long as the corresponding aptamer to each analyte is accessible. Consequently, other than being applied for biochemical sensing in body fluids, such as sweat, saliva, and sputum, OECTs and their relevant sensing systems were implemented into various living plants, including garden rose [34], tomato [35], [36], aspen tree [37], and Venus flytrap [38], to monitor distinct biochemical and bioelectrical signals in vivo.
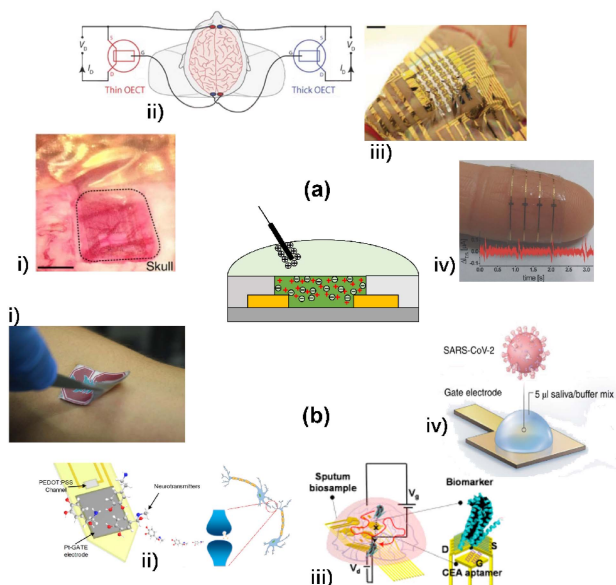
FIGURE 4. (a) OECT for bioelectrical sensing. i) ECoG. [27]. Reproduced with permission, Copyright 2013, Springer Nature. ii) EEG [8]. Reproduced with permission, Copyright 2015, American Association for the Advancement of Science. iii) EMG [24]. Reproduced with permission, Copyright 2016, Wiley-VCH. iv) ECG [28]. Reproduced with permission, Copyright 2014, Wiley-VCH GmbH. (b) OECT for biochemical sensing. i) biomarkers in sweat [26]. Reproduced with permission, Copyright 2019, Wiley-VCH GmbH. ii) catecholamine neurotransmitters (CA-NTs) [39]. Reproduced with permission, Copyright 2020, Elife Sciences Publications. iii) biomarkers in sputum [40]. Reproduced with permission, Copyright 2022, Elsevier. iv) SARS-CoV-2 [33]. Reproduced with permission, Copyright 2021, Springer Nature.

FIGURE 5. (a) Typical circuit diagram of MEA. (b) Photograph to two typical MEAs on flexible substrate and textile, respectively. [49]. Reproduced with permission, Copyright 2015, American Association for the Advancement of Science. [50]. Reproduced with permission, Copyright 2015, Nature Publishing Group. Typical circuit diagram of OECT based passive sensing arrays, where (c) presents each transistors have an individual gate wiring, (d) presents shared gate electrode, and (e) presents shared source and gate electrodes.
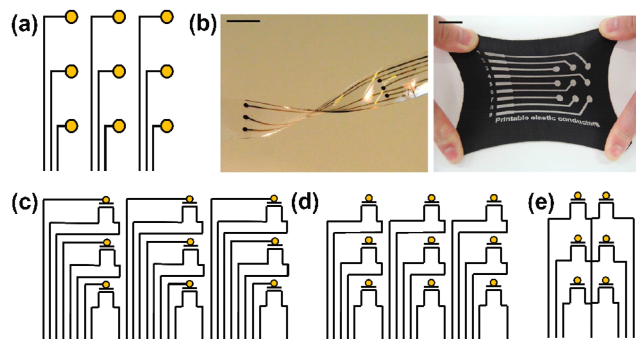
Based on the rapid developments in OMIECs and various sensing applications that OECTs have been employed for, integrated sensing systems based OECTs are further constructed, by integrating various sensors, combining data collecting/processing circuits, and/or portable light-weight power source [24], [41], [42]. Among these systems, sensing arrays consisting of multiple OECTs show extra advantages in high integration levels, good redundancy, low-cost fabrication, and spatiotemporal resolution. In the next section, recent developments in the OECT-based sensing arrays are reviewed.

II. OECT-BASED SENSING ARRAYS
Among all the studied sensing arrays based on OECTs, two major categories they can be classified: passive array and active array. Note, the passive array and active array defined here are not the same as those in flat panel display, which share slightly different names, i.e., passive-matrix and active-matrix [43]. These two kinds of arrays show different advantages and disadvantages, which will be discussed in detail in this section.

A. PASSIVE ARRAYS
Passive arrays are simple in terms of design, and their working principle is straightforward since each sensor is not connected to other sensors in the array (no crosstalk) [44]. Before the

discussion on OECT-based passive arrays, it is worth noting that, well-developed microelectrode arrays (MEA) have been widely studied, where every electrode end in the array act as one sensing terminal [45]. As shown in Fig. 5(a), (b), MEA with good adhesion to human skin, biocompatible design, and excellent stretchability on textile, have been developed and applied in monitoring electrical activity produced by the heart, brain, skeletal muscles, and even cells [46], [47]. There are also many comprehensive reviews summarizing recent advances in MEAs [45]. While for OECT-based passive arrays, one can regard them as an upgraded version of MEAs, where each electrode sensing terminal is replaced by one OECT (or at least the channel of an OECT) (Fig. 5(c)–(e)). Therefore, in an MEA, each electrode sensing terminal typically receives the potential/current variations due to the interaction of the functional electrode with the targeting analyte and transmits the electrical signal out through the electrode wiring. On the contrary, in an OECT-based passive array, targeting analyte would induce variations in the doping state of the channel, due to altered gated potential, or fluctuated ion species/concentrations, et al. Consequently, the change in doping level would be translated to the change on source-drain current (where in most cases, I_D is monitored). This process in OECT-based sensors contains two important stages: 1) Analyte induced sensing process; 2) Transistor induced amplification process. Therefore, compared with MEA, the OECT-based passive array show advantages in low limit of detection, high sensitivity, and typically high signal-to-noise ratio (SNR). Due to these superiorities of OECT-based passive arrays, they have been applied in body fluids sensing [25], [40], and neuromorphic devices [48].

For instance, Xie et al. recently demonstrated an OECT passive array for real-time mapping/monitoring of catecholamine neurotransmitters (CA-NTs) in living rat brains (Fig. 6(a)) [39]. The passive array was fabricated on a polyethylene terephthalate (PET) substrate, where a platinum gate electrode
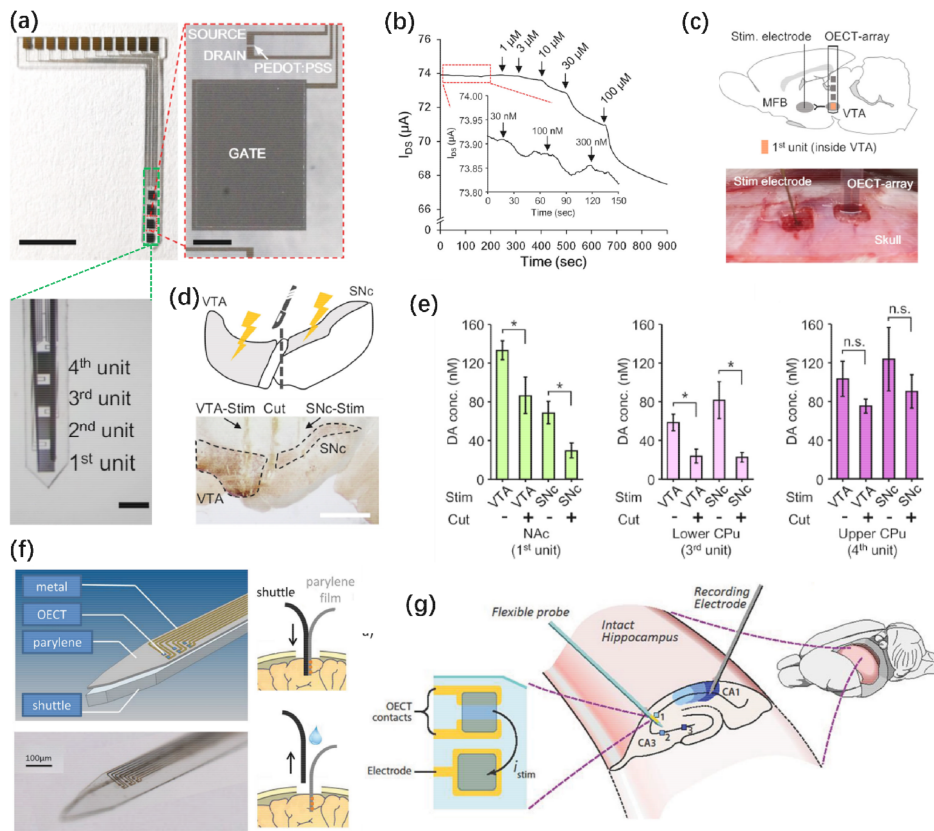
FIGURE 6. (a) Photographs showing the overall (left), enlarged (right), and front (lower) view of the flexible OECT array. Scale bars are 5 mm, 200 mm , and 1 mm for the left, right, and lower panels, respectively. (b) Ex-vivo recording of I_D changes in response to various dopamine concentrations in artificial cerebral spinal fluid containing a high level of ascorbate acid (1.28 mM; $V_D = 0.06$ V; $V_G = 0.6$ V). (c) Schematic diagram (upper) and surgical photogram (lower) of the experimental setup for monitoring in VTA. (d) Schematic diagram of dopamine mapping in the NAc and CPu in response to surgically isolated VTA- or SNc-stimulation (upper panel), and immunohistochemical staining for TH in a brain slice showing the surgical tracks of the stimulation electrode in the VTA or SNc, and the mechanical lesion between these two regions (lower panel). Scale bar, 1 mm. (e) Quantitative analysis of the change in dopamine release pattern at different brain regions across mesolimbic and nigrostriatal pathways, including the NAc, lower CPu, and upper CPu, in response to VTA- or SNc-stimulation before and after the surgical lesion to mechanically break the mutual connections between VTA and SNc. ∗indicates p<0.05 by student t-test; n.s. stands for 'not significant'. "+/-" indicates that the measurements were conducted with/without the VTA-SNc surgical lesion [39]. Reproduced with permission, Copyright 2020, Elife Sciences Publications. (f)Layout of the OECT probe, optical micrograph (bottom panel), and the principle of delamination (right). (g) Stimulating pyramidal neurons in intact hippocampal preparations where pyramidal neurons were recorded from the rightmost section of CA1 along the transverse axis of the hippocampus (dark blue). Correspondingly, pyramidal neurons were stimulated using the OECT, starting from the leftmost section of CA3 [51]. Reproduced with permission, Copyright 2015, Wiley-VCH GmbH.

acts as the sensing electrode towards CA-NTs, while PEDOT: PSS film and gold act as channel and source/drain electrodes, respectively. The utilization of OECT enables a sensitivity of nanomolar range for dopamine detection (Fig. 6(b)). Moreover, such a passive array contains four OECTs with individual electrodes and channels, and is designed with a geometry that can be implanted in the ventral tegmental area (VTA), nucleus accumbens (NAc), and/or caudate putamen (CPu) of a rat brain (Fig. 6(c)). Consequently, due to the special distribution and milliseconds temporal resolution of the OECT array, it allows CA-NT release at different brain regions to be simultaneously monitored, and reveals a complex cross-talk between the mesolimbic and the nigrostriatal pathways (Fig 6(d), (e)). It is believed that the development and application of such an OECT array is a powerful tool for electrochemical analysis in the nervous system and can lead to a wide range of novel neuroscience research.

Moreover, OECT passive arrays can also act as neurotransmitters in the brain. Williamson et al. showed that a seamless interface between the brain and OECT array (4 μm thickness) can be formed due to the adoption of the noninvasive delaminating probes (Fig. 6(f)). Moreover, by penetrating the cortex and stimulating the pyramidal neurons (Fig. 6(g)), both population spikes and action potentials were evoked between stimulus pulses. This work indicates that the OECT array holds great potential for next-generation human-machine/brain-computer interfaces [51]. Note that to mimic neural activities, next-generation human-machine/brain-computer interfaces are required to be able to stimulate individual neurons with minimal negative impact [14]. Thus, these devices must be implanted precisely in the target brain region. While for typical silicon neural probes, to ensure the device does not shift from the ideal implantation path, relatively thick microstructures (10 μm to 200 μm)
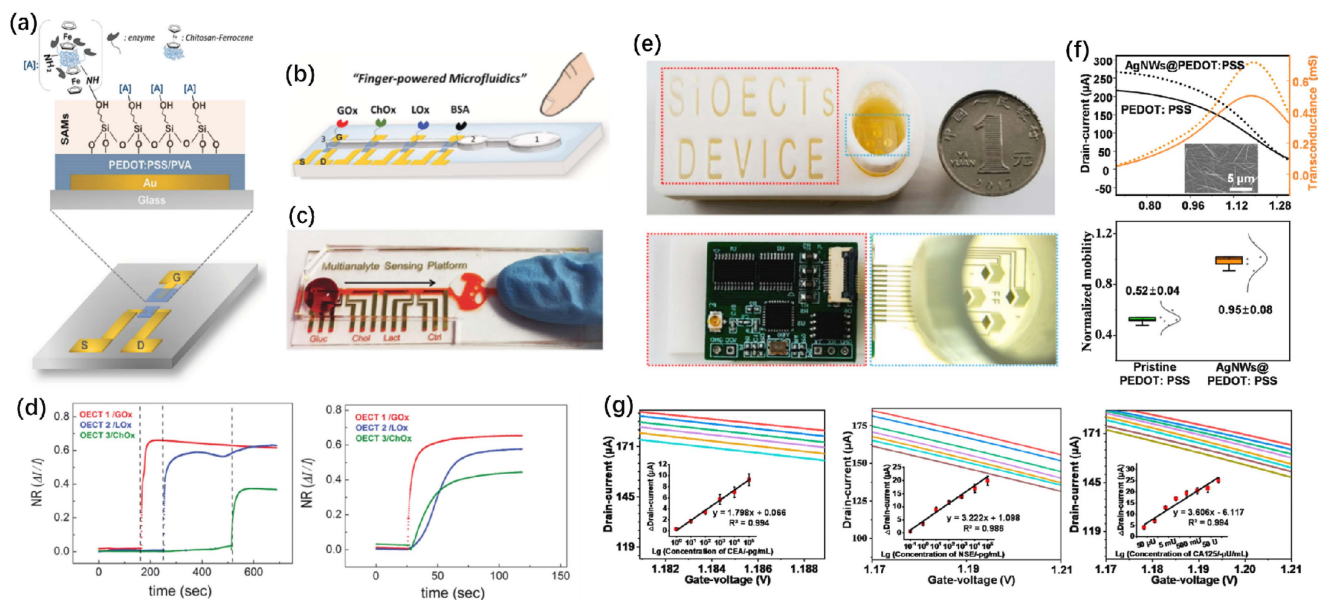
FIGURE 7. (a) Schematic representation of a single OECT device structure where the gate electrode is modified with the specific enzyme. (b, c) Schematic illustration of the OECT array. (d) Drain current response during successive additions of known concentrations of the three analytes (left) or the addition of a mixture of the three analytes(right) [25]. Reproduced with permission, Copyright 2016, Wiley-VCH. (e) Photographic images and exploded views of SiOECTs. (f) Transfer characteristics and corresponding g_m of the SiOECTs with pristine and AgNWs doped PEDOT: PSS channels. (g) Typical CEA, NSE, and CA125 calibration curves of SiOECTs with the regression analysis, and the corresponding inserted plots are the calibration curves of SiOECTs [40]. Reproduced with permission, Copyright 2022, Elsevier.

are adopted [52], [53], [54]. Such a thick probe produces a tremendous mechanical force between the neural tissue and the probe, which could cause an inflammatory response, disrupt neuronal networks, and lead to adverse reactions [14], [55]. While soft nature of most OMIECs and the ultra-thin design of OECT arrays could effectively avoid these problems and lead to a stable and safe human-machine/brain-computer interface.

Other than biochemical sensing and stimulation for brains, OECT passive arrays have also been applied in point-of-care testing. Pappa et al. designed and fabricated a compact biosensing platform to quantitatively monitor glucose, lactate, and cholesterol levels in saliva (Fig. 7) [25]. This platform consisted of an OECT passive array (four individual OECTs) and a pumpless poly (dimethylsiloxane) (PDMS)-based microfluidic, which can drive the collected saliva to the targeting OECT channel and the functional gate electrode. Here, each gold gate electrode coated with a blend of PEDOT: PSS and polyvinyl alcohol (PVA), is immobilized with glucose oxidase (GO_x), lactate oxidase (LO_x), or cholesterol oxidase (ChO_x), for selectively sensing glucose, lactate, and cholesterol, respectively (Fig. 7(b)). While the fourth gate electrode is functionalized with bovine serum albumin (BSA) as control. Benefiting from the passive array architecture, OECTs in the array are electrically isolated from each other, avoiding the electrical crosstalk from the capacitive coupling. Furthermore, the PDMS-based microfluidics allows for laminar flow, ultra-small sample volume, and fast analysis (Fig. 7(c)), which

further enhanced the portability, miniaturization, and automation of the sensing array [56]. Based on the above setup, the passive array shows decent sensing performance simultaneously after successive additions of the corresponding analytes with known concentration (Fig. 7(d)). While, when a mixture containing all analytes is pumped into the OECT array, all three OECTs show obvious variation in I_D, indicating the capability of the sensor to detect all three analytes at the same time (Fig. 7(d)). Note, the varying response time for each OECT may be related to the spatial location of each device, the additions to the metabolite mixture, and the different properties of each enzyme.

Moreover, Zhang et al. demonstrated another noninvasive and portable multi-channel sputum interdigitated organic electrochemical transistors (SiOECTs) array for the medical diagnosis of lung cancer (Fig. 7(e)) [40]. The organic channel of the fundamental OECT consists of AgNWs doped PEDOT: PSS, which enhances the synergistic determination of biomarkers through enhanced g_m and mobility (Fig. 7(f)). The final fabricated device simultaneously enhanced the quantifications of panel biomarkers of carcinoembryonic antigen (CEA), neuron-specific enolase (NSE), and carbohydrate antigen 125 (CA125) with good selectivity and reliability by modifying each gate electrode with the corresponding aptamer. Comparing this diagnostic array with the clinic-used assay, a high correlation coefficient (CEA: $R^2 = 0.963$) was observed. The introduced SiOECTs-based point-of-care testing array can also achieve the improved diagnostic capability
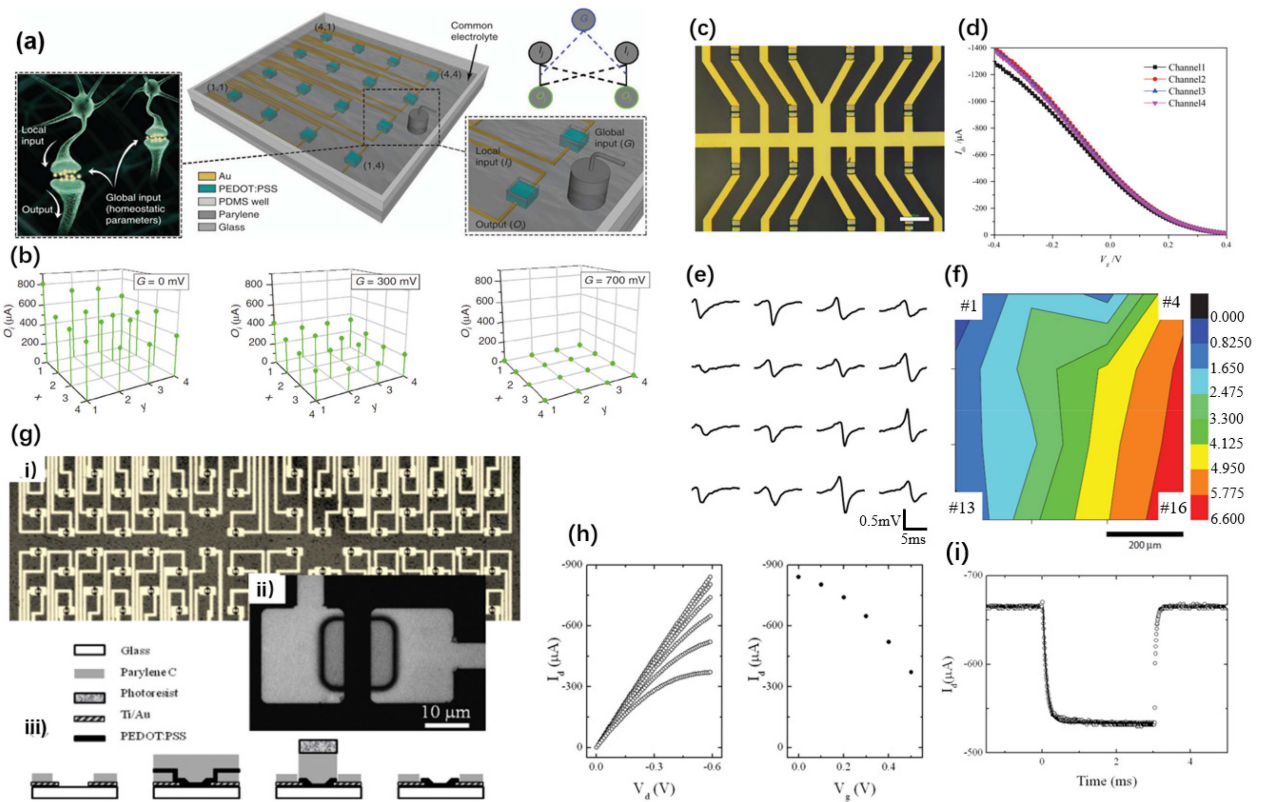
FIGURE 8. (a) Schematic of the configuration of the OECT passive array. Each transistor consists of a PEDOT: PSS channel connected with two Au pads (source and drain electrodes), which provide input I_i and record output O_i. An Ag/AgCl electrode serves as the global input G. (b) Spatial maps showing the variation of outputs O_i when voltages pulses (amplitude of 100mV, width of 50 ms) were used at each local input I_i, and various DC values (0, 300 and 700 mV) were used as a global input [48]. Reproduced with permission, Copyright 2017, Nature Publishing Group. (c) The optical image of a 16 channels OECT array. (d) Transfer curves of the four OECTs in the top left corner of the array. $V_D = $ -0.4 V. (e) A schematic showing the spatial location of action potentials recorded by 16 OECTs. (f) The contour map of local activation time is based on the data in (e). The unit of the color bar is ms [23]. Reproduced with permission, Copyright 2016, Wiley-VCH. (g) Optical images of the high-density OECT array (i), an enlarged single OECT (ii), and the fabrication process of the array (iii). (h) Output and transfer characteristics of one OECT in the array. (i) Temporal response of the I_D of an OECT with 0.4 V V_G pulse [2]. Reproduced with permission, Copyright 2011, American Institute of Physics.

of lung cancer patients as a comparison against healthy individuals with an optimum area under the curve (AUC) of 0.931, a sensitivity of 87.0%, and a specificity of 86.5%. It is expected that this SiOECT-based array can act as a critical platform for the diagnosis of sputum-related diseases.

Except for the above-mentioned OECT-based passive arrays, where every electrode in the array is for one individual OECT, there are other kinds of passive arrays based on OECTs where some of the electrodes are shared with multiple OECTs (Fig. 8). As shown in Fig. 8(a), an OECT passive array based on PEDOT: PSS channel has a global gate electrode, and all the transistors are controlled by this gate electrode through electrolyte [48]. Such setup is similar to and behaves like the homeoplasticty phenomena of the neural network. This 4 × 4 OECT passive array consists of transistors with a square channel configuration of 50 × 50 μm ($L \times W$), where each of the source and drain electrode is for an individual OECT. While the common electrolyte and gate electrode established a complex soft connection between individual transistors, where the transistors can all be controlled simultaneously by the gate bias, the amplitude of the output signal (I_D) depends

on the relative location of the channel and the gate (Fig. 8(b)). While in most previous neuromorphic arrays, where all these devices are connected with a predefined physical wire network, which severely limits the number of connections that can be established between different devices. However, the array illustrated here presented the concept of global regulation, synchronization of I/O transmission, and global clock behavior, where electrolyte connections have significant advantages in achieving a higher level of complex networks of neuromorphic devices.

As mentioned above, due to the high g_m and good biocompatibility, functional cells can be directly cultured on OECT arrays, where their physiological behavior can be detected and monitored. Consequently, Gu et al. fabricated a 16-channel OECT array, where all the OECTs share a common source electrode, while each OECT processes one particular drain electrode (Fig. 8(c)) [23]. After culturing a primary rat cardiomyocyte monolayer on the array, the action potentials of these cells are monitored subsequently. Large g_m with a peak value of 2.5 mS and good SNR between 4 – 10 of the OECTs in the array lead to effective sensing and amplification

Capabilities (Fig. 8(d)). Therefore, cardiac electrophysiology such as the heartbeat frequency, direction, and velocity of the propagation of action potentials, the action potential duration, and action potential rise time, is acquired in a two-dimensional scale by such a passive array, enabling quantitatively investigation of the action potential characteristics (Fig. 8(e), (f)). Moreover, irregular action potential propagation on a rat cardiomyocyte model, which is similar to conduction disorder, can be reproduced. Furthermore, such an array can record cell action potentials for 42 days without significant signal attenuation. Accordingly, this OECT array not only showed good stability in a long-term cell cultures environment but also excellent biocompatibility. Long-term monitoring is crucial for future studies of human cardiac cells, thus, the capability of the OECT array is favored for heart disease research and drug screening.

OECT passive array with a common gate electrode for physiological sensing can also be integrated with high device density, where Khodagholy et al. demonstrated a general process for the miniaturization of OECTs by adopting photolithography and lift-off processes (Fig. 8(g)) [2]. Specifically, such passive array fabrication was assisted with a 2 μm thick parylene C (a biocompatible material with good dielectric properties and biocompatibility) film coating. Thus, the arrays would lead to less invasive manners with living cells and also protect from the swelling and undesired side reactions when interacting with the aqueous environment. Overall, this passive array consists of 64 OECTs with L of 6 μm and adjacent channel center to center distance of 85 μm. Representative OECT performance (including output and transfer characteristics) indicates an effective doping/dedoping process in the PEDOT: PSS channel. Besides, the response time of this OECT array is about 100 μs with a low operating voltage of 0.4 V, indicating reduced parasitic capacitance contribution. Such high-density OECT passive arrays may be suitable for the monitoring of electrically active cells and various biosensing applications where high spatiotemporal resolution is required [2].

Other than biosensing-related applications, OECT arrays can also be utilized for the construction of functional circuits, which enables tremendous development potential in the area of the Internet of Things (IoT) [57], [58].

B. ACTIVE ARRAYS

Compared with passive arrays, OECT based active sensing array consists of individual OECTs that share their source and drain wires with other OECTs in the same column/row, which is similar to that of the active matrix in flat panel displays (Fig. 9). In an active matrix, each pixel/sensor consists of at least one transistor. Due to the introduction of transistors in the crossbar geometry, active array and active matrix exhibit obvious advantages in reduced power dissipation, high spatiotemporal resolution, and minimal signal crosstalk [45], [59]. Active arrays have been applied for the sensing/mapping of pressure, temperature, light, magnetic field, and bio-signals
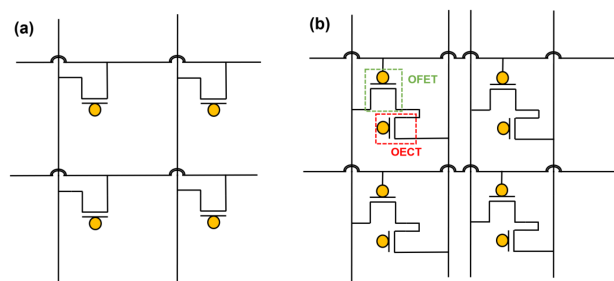

FIGURE 9. Schematic diagram of the OECT active array with (a) one transistor and (b) two transistors under one sensing cell.

[59]. While OECT-based active sensing arrays are mainly employed in physiological sensing/mapping.

Similar to the development of MEA and OECT-based passive arrays, OECT-based active arrays have been widely applied for research related to active/inactive cell location, neural signal detections, and neuron network mappings [60], [61]. Especially, high resolution of electrophysiological signal monitoring in vivo became a critical topic in elucidating physiological functions, where sensing arrays will need to be not only biocompatibility but also flexible/stretchable. Only in this way, it can be introduced into living animals to monitor their health status with minimum side effects. Typically, substrate and electrode materials for OECTs possess a high Young's modulus (>10 GPa), so it is challenging to attach OECTs with hard materials to bio-surfaces where dynamically moving and surgical bleeding exist. For instance, the surface of a heart would be damaged in contact with such "hard" devices. Someya et al. incorporated honeycomb grid substrate with OECT active array, and realized decent stretchability and biocompatibility, simultaneously (Fig. 10) [62]. By assembling source/drain electrodes on the honeycomb grid, along with the PEDOT: PSS channel and a 100 nm thick poly(3-methoxy propyl acrylate) (PMC3A) encapsulation/interfacing layer (Fig. 10(b)), such 4 × 4 OECT active array shows high g_m of ~1 mS with a total thickness of only 2.6 μm. Here, PMC3A holds antithrombotic properties and excellent ionic conductivity, which allows the OECT array exhibits long-term electrocardiographic (ECG) monitoring in a bleeding environment, while only leading to less than 2% variation on electrical properties and response time of the OECTs after 10 hours measurement. As shown in Fig. 10(d), when elongation strains applied on the array increase from 0% to 15%, stable transfer characteristics and g_ms are obtained, which reveal good performance resistance to stretching. When attached such an active array to the exposed surface of the rate heart (Fig. 10(e)), along with a proper circuit driving setup, the spatial distribution of the recorded ECG can be observed. Specifically, the spatial-temporal distribution of the ECGs on the heart surface reveals the working condition of the rat heart (Fig. 10(f)). Such an OECT active array with both good stretchability and operational stability can be applied in other biosensing fields where mechanical conformability and biocompatibility are required.
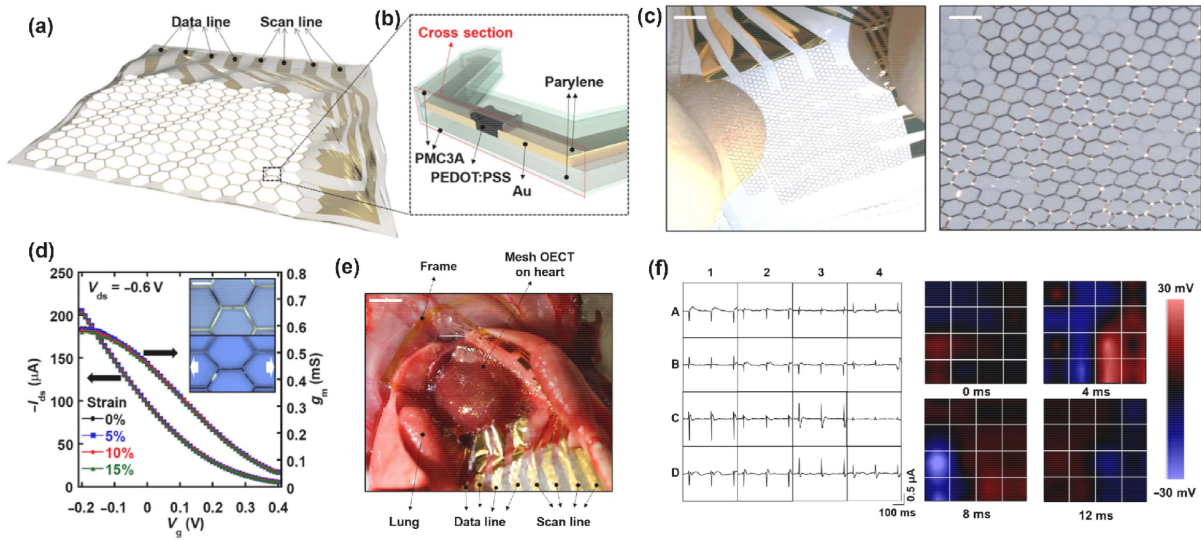
FIGURE 10. (a) Illustration of the stretchable OECT active array on a honeycomb grid parylene substrate. (b) Cross section of one stretchable OECT in the array. (c) Optical image of stretched 4 × 4 OECT active arrays (Scale bar, 3 mm) along with a magnified view of the array (Scale bar, 500 μm). (d) Transfer and g_m curves of a single OECT under 0, 5, 10, and 15% stretching strains. Inset: Microscope image of a single OECT, which is stretched with 10% strain. Scale bar, 200 mm. (e) Photograph of the stretchable OECT array on the heart of a rat. Scale bar, 5 mm. (f) ECG signals from multiplexed 4 × 4 OECT array (V_D = -0.3 V), along with the time delay of ECG signals [42]. Reproduced with permission, Copyright 2018, American Association for the Advancement of Science.
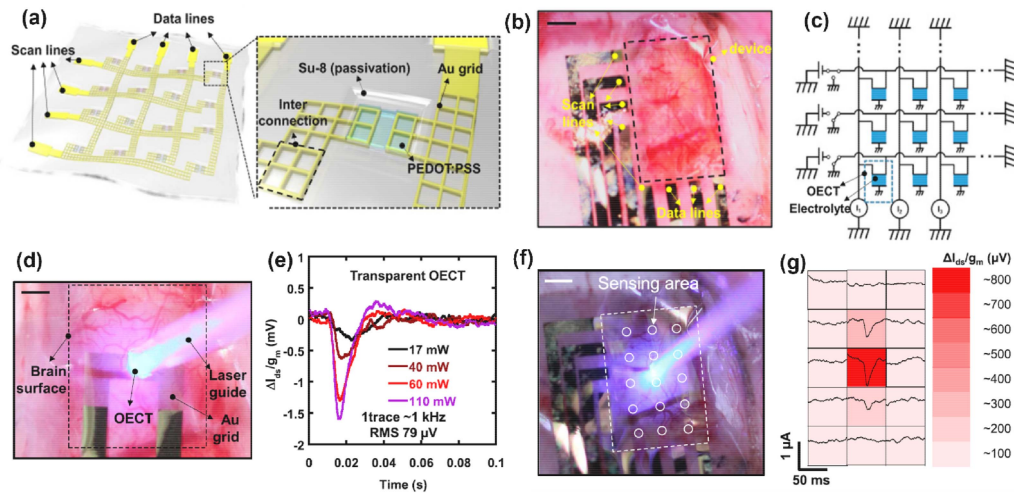
FIGURE 11. (a) Illustration of the transparent OECT active array with a magnified image of a single transparent OECT. (b) Photo of the 3 × 5 transparent OECT array (black dashed square) on the cortical surface of an optogenetic rat. Scale bar: 1 mm. (c) Schematic circuit diagram of the OECT array. A certain voltage was applied to the drain line to be measured. The other lines were all connected to the ground of the circuit for preventing cross-talk. The source lines were connected to each current meter. (d) Photograph of the transparent OECT on a neuron-concentrated area of the cortical surface of an optogenetic rat with blue laser continuous stimulation. Scale bar: 500 μm. (e) The recorded signal by transparent OECT under light stimulation of a 475-nm wavelength. (f) Photograph of the transparent array in a neuron-concentrated area on the cortical surface of an optogenetic rat with blue laser continuous stimulation. Scale bar: 1 mm. (g) Spatial distribution of the brain signal intensity measured by the 3 × 5 transparent array [41]. Reproduced with permission, Copyright 2017, National Academy of Sciences.

On the other hand, optical observation and light stimulation on bio-tissues that are covered by the sensing array is extremely important and useful, especially in the area of optogenetics. Moreover, the OECT array with optical transparency helps the precisely installation of the sensing array at the location of interest and allows optical microscopy

to observe biological tissues directly [51], [63]. Therefore, OECT active array with high optical transparency is fabricated by introducing a 1.2 μm Parylene-C substrate and micropatterned transparent Au grid wirings with a linewidth of 3 μm (Fig. 11(a)) [41]. 60% transparency to 475 nm light wavelength was achieved, which allows direct blue laser
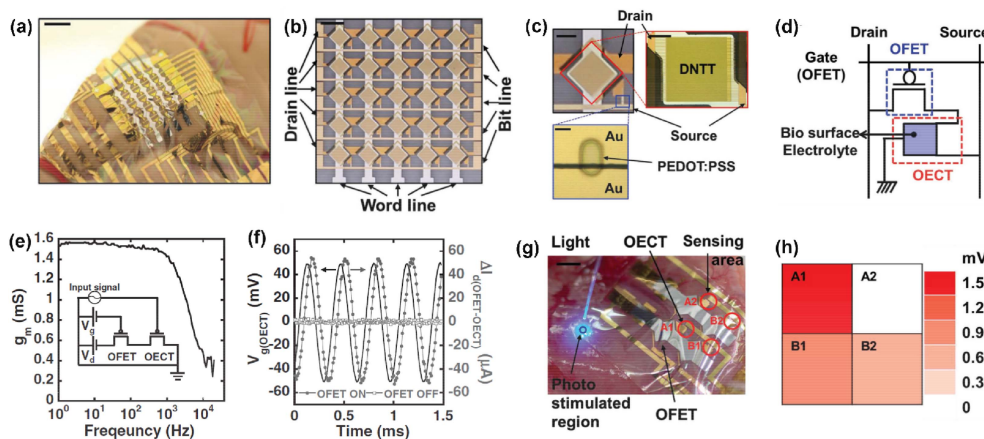
FIGURE 12. (a) Photograph of a 5 × 5 active array on a curved surface (Scale bar; 0.5 cm). (b) Top-view photograph of the 1 × 1 cm² sensor array (Scale bar; 2 mm). (c) Detailed view of an individual pixel together with the OFET and the OECT (Top left, Scale bar; 0.5 mm), without the OECT (Top right, Scale bar; 0.2 mm), and without the OFET (Bottom, Scale bar; 5 μm). (d) Schematic circuit diagram of the single sensing spot. (e) Frequency dependence of the g_m of the OECT. (f) I_D-time curve of the 3 kHz oscillation with a 50 mV peak-to-peak when the OFETs were ON and OFF. (g) Photograph of a 2 × 2 array on muscle tissue (Scale bar; 2 mm). (h) The spatial distribution of the myoelectric signal intensity was measured by the 2 × 2 array [24]. Reproduced with permission, Copyright 2016, Wiley-VCH.

stimulation on the tissue that is covered by the array (Fig. 11(b)). This 3 × 5 OECT active array with a total thickness of 3 μm shows an average g_m of 1.1 mS and a response time of only 363 μs. By driving the array with a customized circuit, cross-talk between transistors can be effectively eliminated (Fig. 11(c)). When a laser stimulation is applied on the cortical surface of a rat under a transparent OECT, the transistor responses with obvious variation on I_D where higher stimulation light intensity leads to a stronger amplitude of I_D variation (Fig. 11(d), (e)). When using the 3 × 5 transparent OECT active array with 1 mm² resolution, the array can reflect the location of the laser simulation easily (Fig. 11(f), (g)), which indicates that the transparent, stable, and ultra-flexible array show tremendous potential in complex studies on optogenetics and other related applications.

Except for the above-mentioned transistor configuration in the active array, the OECT array with two transistors under one sensing cell has also been investigated by Lee et al. [24]. Such configuration can control each sensing spot more precisely and easily even though the complexity of the array is increased compared to the above two active arrays. Moreover, high SNR along with high spatiotemporal resolution can also be integrated into this active array, which satisfies the requirements for the detection of various electrophysiological signals, including neurons and cardiomyocytes [64], [65], [66]. The developed 5 × 5 arrays are composed of OECTs and organic field-effect transistors (OFETs) with the characteristics of ultra-flexible and high temporal resolution (Fig. 12(a), (b)). Unlike the above-mentioned OECT active arrays, this sensing array contains one OECT and one OFET under each detection cell, where OFET acts as the control transistor to switch on or off the sensing unit, while OECT act as the sensor (Fig. 12(c), (d)). Here, OFETs have good mechanical durability and flexibility, which form decent mechanical contact with curved biological surfaces [67].

While for OECTs, owing to their large g_m, they are naturally suitable for small electrophysiological signal detection. The developed integrated sensing unit shows a cut-off frequency (f_c) of more than 10^3 Hz and can trace and amplify the input voltage (50 mV peak-to-peak) with an oscillation frequency of 3 kHz (Fig. 12(e), (f)). Therefore, a 2 × 2 sensing array is placed on a gracilis muscle covering both light-activated and non-activated muscle areas (Fig. 12(g)), where the distribution of activated areas is successfully mapped by the array with good SNR.

From the above-mentioned results, it is quite obvious that the OECT array can monitor extracellular potential effectively. However, intracellular action potential recording is largely limited to three-dimensional MEA strategies, which severely prohibited the implementation of organic electronics. Jimbo et al. found that adjusting the driving voltage of the OECT array can cause electroporation where the array can record intracellular cation potential [68]. A 4 × 4 OECT active array with a precisely defined geometry and channel dimension is fabricated and cultured with human-induced pluripotent stem cell-derived (hiPSC-derived) cardiomyocytes (Fig. 13(a)-(c)). A DC/pulse voltage supply was applied to the drain electrode connected lines (Data lines), while scan lines were all connected to the ground. When a DC drain voltage is applied, almost no voltage bias variation is generated between the channel and the gate electrode, thus the extracellular field potential is recorded. However, when a pulse drain voltage is applied, high-frequency voltage differences exist between the channel and the gate electrode. Consequently, a large electrical field is applied to the cell, which causes electroporation, and the intracellular action potential can be recorded thereafter (Fig. 13(d)). Moreover, it is also demonstrated that the effect of electroporation could be controlled by tuning the geometry and driving the voltage of OECTs.
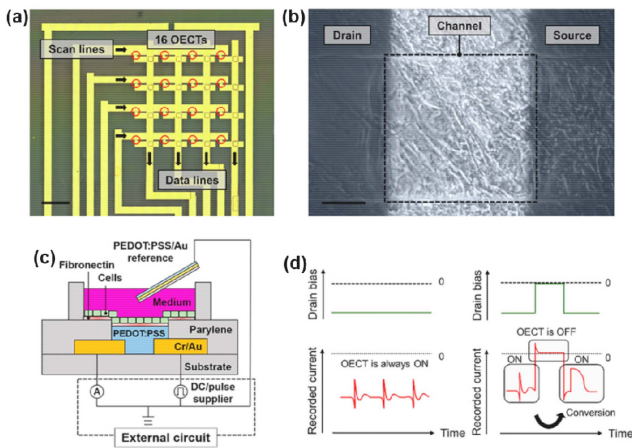
FIGURE 13. (a) Top-view photograph of a 4 × 4 OECT array, where each channel (red circle) is placed at a 2 mm spacing. (Scale bar, 2 mm) (b) hiPSC cardiomyocytes cultivated on a channel (Scale bar, 100 μm). (c) Cross section of the structure and circuit configuration of an OECT where cells are cultured. (d) Drain currents are recorded by OECT with a DC drain voltage or with a pulse drain voltage. On applying a pulse drain voltage, a high-frequency component flows from the drain to the reference electrode causing electroporation, and thus the intracellular action potential is recorded [68]. Reproduced with permission, Copyright 2021, National Academy of Sciences.

III. PERSPECTIVES ON OECT-BASED SENSORS AND SENSING ARRAYS

From the above discussion, it is inspiring to see that OECT-based sensing arrays can be applied in various physiological signal detection/mapping. However, to take full advantage of OECT-based sensing arrays, several critical aspects related to OECTs and their sensors, require special attention, which include stability, bandwidth, integration density, and power dissipation.

A. STABILITY

Stability is one of the most critical factors for any electronics, while this is particularly important for OECTs and their related arrays. With the fast development and increasing demand of the biosensor market, long-term monitoring of physiologic signals is of paramount importance, which not only requires the sensors can be ultra-stable during storage, but also to maintain stable output during long-term bias (could be voltage bias, current bias, or both). Previous studies have revealed that the cycling stability of OECTs is quite limited due to the underlying working mechanism of such transistors. Specifically, OMIECs conduct both ions and electrons, while the conducting of ions would typically lead to swelling of OMIECs, and variations in microstructure [69]. Moreover, side reactions during the electrochemical process due to over-shooting of the bias voltage or impurities in OMIECs and/or electrolytes could continuously consume active materials in OECTs.

For instance, as the most commonly used channel in OECTs, PEDOT: PSS has high conductivity (∼3000 S/m) but limited electrochemical stability in an aqueous solution

[70], [71], [72], [73]. By introducing dodecylbenzene sulfonic acid (DBSA) and GOPS, PEDOT: PSS-based OECTs demonstrated stable performance for more than three weeks [12]. The high stability of such PEDOT: PSS is attributed to the crosslinked matrix, which prevents the negative effect from swelling [14]. Moreover, as illustrated in Fig. 3(c), (d), redistributing the side chains of polymer can also control the swelling effect and lead to OECTs with high cycling stability [22].

As mentioned above, non-capacitive faradaic side reactions affect the electrochemical redox stability of OMIECs [14], where the reaction between the OMIEC and the electrolyte may modify OMIEC's chemical composition [74]. Backbone structure can effectively tune the redox stability of OMIECs. For instance, Giovannitti et al. synthesized a copolymer based on pyridine-flanked DPP with 33′-methoxybithiophene (p(gPyDPP-MeOT2)) and showed enhanced cycling and bias stability when compared with PEDOT: PSS and p(g2T-TT) due to lowered energy level and eliminated the generation of reactive side-product hydrogen peroxide [75].

On the other hand, due to the requirement for flexibility, and even stretchability on the OECTs and their related arrays, performance stability under mechanical strain has to be considered, especially for applications on deformable surfaces. Other than the above-mentioned strategies by introducing ultra-thin OECT geometry [24], [41], [42], [68], micro/nano structure engineering on the OECT channel provides an alternative way. For instance, Chen et al. introduced an ultra-stretchable and electrochemically redox stable OECTs with combination of an amphiphilic semiconducting (25-bis(2-octyl dodecyl)- 36-di(thiophene-2-yl)-25-diketo-pyrrolopyrrole-alt-25-bis(3- triethyleneglycoloxy-thiophen-2-yl) (DPP-g2T) and a biaxially pre-stretched film/device architecture [76]. These OECTs exhibit stable electrochemical and mechanical performance with increasing tensional strain up to 140% by introducing honeycomb microstructure in the channel. Such high-performance OECT, which can maintain stable sensing and signal output under strains, is suited for ECG monitoring, synapse simulation, and other bio-related applications.

B. EFFECTIVE BANDWIDTH

High f_c is another critical parameter of OECTs and their related arrays, for biological sensing. Assuming the average voltage drop between the OMIEC and the gate electrode ($\Delta V = V_G - 0.5V_D$) and the transient behavior is consistent with steady-state characteristics. The transient behavior for a simplified OECT where (de)doping occurs everywhere within the OMIEC without saturation effects can be described as [7]:

$$I(t, V_G) = I_{SS}(V_G) + \Delta I_{SS}(1 - f(\tau_e/\tau_i))\exp(-t/\tau_i) \quad (3)$$

where $I_{SS}(V_G)$ is the steady-state source-drain current at V_G, ΔI_{SS} is the source-drain current difference at steady-state V_G and $V_G = 0$ V, τ_e and τ_i are the electronic and ionic transit times, respectively. The character of the equation above is dominated by the ratio $\tau_e/\tau_i \sim lL^2/\mu V_D$, where l is the distance

from the organic film to the gate electrode. From this relationship, the character of the transient response depends on the gate electrode location, L, and V_D [7]. While in typically OECTs, the short channel makes the variation of transient time depends more on τ_i, not to mention that Eq. (3) ignore the contribution from the thickness of the OMIECs. Therefore, the operating frequency of OECTs, i.e., transient behavior, is mainly affected by the diffusion efficiency of ions between the electrolyte and the OMIEC bulk. Based on this conclusion, George et al. introduced an internal ion-gated organic electrochemical transistor (IGT), which combines PEDOT: PSS with d-sorbitol [77]. This blend maintains ions within the channel, creating a self-(de)doping process. Consequently, ions do not need to transfer from electrolyte to organic semiconductor film, thus, reducing the distance that ions travel during the (de)doping process. The transient time for this IGT is decreased to only 2.6 μs (an effective bandwidth of 380 kHz). Moreover, since the switching speed of OECTs is inverse proportional to L. Vertical OECTs (vOECTs), which is advantageous for achieving short channel, inherently can exhibit short transient time [14]. Donahue et al. [78]. demonstrated vOECTs with PEDOT: PSS, which exhibited reduced footprint along with high f_c between 1.3 and 1.7 kHz for $L = 450$ nm.

C. INTEGRATION DENSITY

High integration density is required for the OECT array to yield a high spatiotemporal resolution. Especially, neurons in the brain are organized in a complicated pattern, and well-developed MEA for ECoG monitoring typically shows ultra-high integration density to obtain the required resolution [79]. For example, Gholizadeh et al. [80]. demonstrated a high-density vertically aligned carbon nanotube nanoelectrode array (VACNT-NEA) with glutamate dehydrogenase covalently attached to the CNT tips as electrochemical glutamate biosensors, which exhibited an extremely low detection limit of 10 nM for glutamate. Liu et al. [81]. reported a high-density vertical Si nanowire array ($\sim$62500 tips/mm^2) with independent electrical addressability and high spatial resolution. These arrays were utilized to record electrophysiological signals from primary neurons of rat/mouse and hiPSC-derived neurons without cell damage [82]. However, in terms of OECT-based arrays, the highest density is limited at about 950/mm^2 [2], which is far too low compared to these in MEA. While the development of a high-density OECT array can borrow the design/fabrication experiences of MEAs.

On the other hand, current processing techniques for sensor fabrication on 1-10 μm scales are still challenging, especially on soft substrates and for organic functional materials. Specifically, uniformity of functional materials coating decreases along with thickness/length scale, and irregular morphologies may create inconsistency in sensor performance, which is vital for array fabrication. Moreover, due to the mismatched Young's modulus of different materials/layers, concentrated stress in devices could lead to mechanical fracture and result in the failure of any electronics. Consequently, the footprint of the current OECT-based arrays tends to be quite large/bulky [79].

While regarding the two types of OECT arrays, even though passive arrays exhibit no/minimal crosstalk and higher f_c when driving the whole array, they require extensive wiring (each transistor has its own source/drain connections and does not share with other transistors) and connection portals with driving circuits (Fig. 5). This kind of setup would be problematic when a large amount of sensing cells is needed. While for OECTs-based active matrix, since all the source and drain electrodes/wires are shared with other transistors that are in the same column/row, the integration of the active array can be much denser (Fig. 9). Furthermore, an array based on vOECTs can be integrated with an even higher density, since their source/drain electrodes act as interconnector and contacting pads at the same time. The above merit demonstrated that an active array is suitable for minimizing the size of each sensor cell and simultaneously allows for higher density and higher resolution [83].

D. POWER DISSIPATION

Fast developing portable and wearable electronics require low power dissipation. As one of the most important components of these electronics, sensors, especially emerging sensing arrays with low power consumption, are highly desired and mandatory. For OECT-based sensing arrays, high power dissipation in each transistor will irreversibly affect the stability of the sensing system, and also lead to local temperature elevation, which would cause a severe negative impact on the bio-tissues in contact with the sensing array.

Even though OECT holds ultra-low driving voltage that can be lower than 1 V, the capacitance and I_D can be higher than conventional transistors. Therefore, proper control of the capacitance of the electrolyte and current restriction needs to be considered. Moreover, as sensing transistors, they are preferred to be biased under the voltage where the largest g_m is yielded, thus leading to the highest amplification capability. Consequently, controlling the peak g_m to be at around $V_G = 0$ V is a simple but practical way to achieve low power dissipation.

In traditional Si technology, complementary circuits are widely applied due to their low power dissipation, excellent noise immunity, and simple circuit design [84]. Here, OECT sensing arrays combined with complementary circuits are also investigated for the reduction in power consumption. Note, research on complementary circuits in the area of organic electronics is mostly based on organic TFTs [85]. While complementary circuits based on OECTs are only reported in recent years due to the unbalanced performance of p-type and n-type OECTs. Note, most of the reported high-performance OECTs are based on p-type OMIECs, while the development of comparable n-type OECTs is lagging due to much lower g_m and inferior electrochemical redox stability [86], [87]. Even though the development in this area is limited, there are several representative studies

on OECT-based complementary circuits that have demonstrated the advantages of low power dissipation and high sensitivity [88], [89]. For instance, Sun et al. showed one of the first complementary inverters based on OECTs by using poly(benzimidazobenzophenanthroline) (BBL) based n-type OECTs and poly(3-carboxy-pentyl-thiophene) (P3CPT) based p-type OECTs [87]. BBL, as a fully conjugated ladder-type polymer with double bonds lock-in rigid backbone conformation, has emerged as a high-performance and air-stable n-type OMIECs [90], where high electron mobility could be achieved by simultaneously improving the local aggregation and interconnectivity of domains. Therefore, an inverter based on such advanced materials could operate at a supply voltage of 0.6 V, with relatively high voltage gain (> 11), and a sizeable worst-case noise margin (NM) of 0.2 V. Although the above inverter could be used as amplifying transducers to enhance the recorded signal of a biological event with low power consumption, BBL based n-type OECT has a $\mu C*$ that is 1-2 orders lower than that in PEDOT: PSS based p-type OECTs. Since $C*$ of BBL is 20 times higher than PEDOT: PSS, the electron mobility of BBL is thus four orders lower than that of PEDOT: PSS [86]. Therefore, high-performance n-type OMIECs are still challenging, and later research should focus more on new material design/synthesis where an interchain coupling in the aggregates and/or delocalized states can be facilitated [91].

IV. SUMMARY AND OUTLOOK

This review summarizes recent advances in OECT based sensing arrays and discusses critical aspects related to OECTs and their sensors. Owing to the advantages in flexibility/stretchability, high sensitivity, and biocompatibility of OECT arrays, they have been applied in a wide range of novel applications related to biosensing/bio-interfacing. Current studies revealed that due to the mixed ionic-electronic working mechanism of such transistors, stability is one key obstacle them need to overcome, while high precision fabrication technique for OECTs is urgently required for microscale and high-density integration. Moreover, lagged development of n-type OECTs also limits the development of high performance OECT array with better sensitivity and lower power dissipation. In general, the emerging studies on OECTs have added new possibilities on transistor-based sensing technologies, and the introduction of OECT-based sensing array has brought extensive potentials for the advancement of healthcare biotechnology.

ACKNOWLEDGMENT

REFERENCES

[1] R. G. Arns, "The other transistor: Early history of the metal-oxide semiconductor field-effect transistor," *Eng. Sci. Educ. J.*, vol. 7, no. 5, pp. 233–240, 1998.

[2] D. Khodagholy et al., "High speed and high density organic electrochemical transistor arrays," *Appl. Phys. Lett.*, vol. 99, no. 16, 2011, Art. no. 163304.

[3] E. Zeglio and O. Inganas, "Active materials for organic electrochemical transistors," *Adv. Mater*, vol. 30, no. 44, Nov. 2018, Art. no. e1800941.

[4] R. B. Rashid, X. Ji, and J. Rivnay, "Organic electrochemical transistors in bioelectronic circuits," *Biosens Bioelectron*, vol. 190, Oct. 2021, Art. no. 113461.

[5] M. J. Panzer and C. D. Frisbie, "Polymer electrolyte-gated organic field-effect transistors: Low-voltage, high-current switches for organic electronics and testbeds for probing electrical transport at high charge carrier density," *J. Am. Chem. Soc.*, vol. 129, no. 20, pp. 6599–6607, May 2007.

[6] J. Rivnay, S. Inal, A. Salleo, R. M. Owens, M. Berggren, and G. G. Malliaras, "Organic electrochemical transistors," *Nature Rev. Mater.*, vol. 3, no. 2, 2018, Art. no. 17086.

[7] D. A. Bernards and G. G. Malliaras, "Steady-state and transient behavior of organic electrochemical transistors," *Adv. Funct. Mater.*, vol. 17, no. 17, pp. 3538–3544, 2007.

[8] J. Rivnay et al., "High-performance transistors for bioelectronics through tuning of channel thickness," *Sci. Adv.*, vol. 1, no. 4, May 2015, Art. no. e1400251.

[9] D. Khodagholy et al., "High transconductance organic electrochemical transistors," *Nat. Commun.*, vol. 4, no. 1, 2013, Art. no. 2133.

[10] M. Stephen et al., "Crown ether enabled enhancement of ionic–electronic properties of PEDOT: PSS," *Mater. Horiz.*, vol. 9, no. 9, pp. 2408–2415, 2022.

[11] M. Asplund, T. Nyberg, and O. Inganas, "Electroactive polymers for neural interfaces," *Polym. Chem.*, vol. 1, no. 9, pp. 1374–1391, 2010.

[12] M. ElMahmoudy, S. Inal, A. Charrier, I. Uguz, G. G. Malliaras, and S. Sanaur, "Tailoring the electrochemical and mechanical properties of PEDOT:PSS films for bioelectronics," *Macromol. Mater. Eng.*, vol. 302, no. 5, May 2017, Art. no. 1600497.

[13] A. Håkansson et al., "Effect of (3-glycidyloxypropyl)trimethoxysilane (GOPS) on the electrical properties of PEDOT:PSS films," *J. Polym. Sci. Part B: Polym. Phys.*, vol. 55, no. 10, pp. 814–820, 2017.

[14] A. Nawaz, Q. Liu, W. L. Leong, K. E. Fairfull-Smith, and P. Sonar, "Organic electrochemical transistors for in vivo bioelectronics," *Adv. Mater*, vol. 33, no. 49, Dec. 2021, Art. no. e2101874.

[15] C. B. Nielsen et al., "Molecular design of semiconducting polymers for high-performance organic electrochemical transistors," *J. Am. Chem. Soc.*, vol. 138, no. 32, pp. 10252–10259, Aug. 2016.

[16] M. Abarkan et al., "Vertical organic electrochemical transistors and electronics for low amplitude micro-organ signals," *Adv. Sci. (Weinh)*, vol. 9, no. 8, Mar. 2022, Art. no. e2105211.

[17] T. Lei, J.-Y. Wang, and J. Pei, "Roles of flexible chains in organic semiconducting materials," *Chem. Mater.*, vol. 26, no. 1, pp. 594–603, 2013.

[18] J. G. Mei and Z. N. Bao, "Side chain engineering in solution-processable conjugated polymers," *Chem. Mater.*, vol. 26, no. 1, pp. 604–615, Jan. 2014.

[19] Y. Yang, Z. Liu, G. Zhang, X. Zhang, and D. Zhang, "The effects of side chains on the charge mobilities and functionalities of semiconducting conjugated polymers beyond solubilities," *Adv. Mater*, vol. 31, no. 46, Nov. 2019, Art. no. e1903104.

[20] B. Meng, J. Liu, and L. X. Wang, "Oligo(ethylene glycol) as side chains of conjugated polymers for optoelectronic applications," *Polym. Chem.*, vol. 11, no. 7, pp. 1261–1270, Feb. 2020.

[21] A. Giovannitti et al., "Controlling the mode of operation of organic transistors through side-chain engineering," *Proc. Natl. Acad. Sci. USA*, vol. 113, no. 43, pp. 12017–12022, Oct. 2016.

[22] M. Moser et al., "Side chain redistribution as a strategy to boost organic electrochemical transistor performance and stability," *Adv. Mater.*, vol. 32, no. 37, Sep. 2020, Art. no. 2002748.

[23] X. Gu, C. Yao, Y. Liu, and I. M. Hsing, "16-Channel Organic electrochemical transistor array for in vitro conduction mapping of cardiac action potential," *Adv. Healthc Mater*, vol. 5, no. 18, pp. 2345–2351, Sep. 2016.

[24] W. Lee et al., "Integration of organic electrochemical and field-effect transistors for ultraflexible, high temporal resolution electrophysiology arrays," *Adv. Mater*, vol. 28, no. 44, pp. 9722–9728, Nov. 2016.

[25] A. M. Pappa et al., "Organic transistor arrays integrated with finger-powered microfluidics for multianalyte saliva testing," *Adv. Healthc Mater*, vol. 5, no. 17, pp. 2295–2302, Sep. 2016.

[26] S. T. Keene, D. Fogarty, R. Cooke, C. D. Casadevall, A. Salleo, and O. Parlak, "Wearable organic electrochemical transistor patch for multiplexed sensing of calcium and ammonium ions from human perspiration," *Adv. Healthcare Mater*, vol. 8, no. 24, Dec. 2019, Art. no. e1901321.

[27] D. Khodagholy et al., "In vivo recordings of brain activity using organic transistors," *Nature Commun.*, vol. 4, no. 1, pp. 1–7, Mar. 2013.

[28] A. Campana, T. Cramer, D. T. Simon, M. Berggren, and F. Biscarini, "Electrocardiographic recording with conformable organic electrochemical transistor fabricated on resorbable bioscaffold," *Adv. Mater*, vol. 26, no. 23, pp. 3874–3878, Jun. 2014.

[29] G. Buzsaki, *Rhythms of the Brain*. London, U.K.: Oxford Univ. Press, 2006.

[30] S. Jadoon et al., "Recent developments in sweat analysis and its applications," *Int. J. Anal. Chem.*, vol. 2015, 2015, Art. no. 164974.

[31] A. Koh et al., "A soft, wearable microfluidic device for the capture, storage, and colorimetric sensing of sweat," *Sci. Transl. Med.*, vol. 8, no. 366, 2016, Art. no. 366ra165.

[32] R. D. Munje, S. Muthukumar, B. Jagannath, and S. Prasad, "A new paradigm in sweat based wearable diagnostics biosensors using Room Temperature Ionic Liquids (RTILs)," *Sci. Rep.*, vol. 7, no. 1, pp. 1–12, 2017.

[33] K. Guo et al., "Rapid single-molecule detection of COVID-19 and MERS antigens via nanobody-functionalized organic electrochemical transistors," *Nat. Biomed. Eng.*, vol. 5, no. 7, pp. 666–677, Jul. 2021.

[34] E. Stavrinidou et al., "Electronic plants," *Sci. Adv.*, vol. 1, no. 10, Nov. 2015, Art. no. e1501136.

[35] N. Coppede et al., "An in vivo biosensing, biomimetic electrochemical transistor with applications in plant science and precision farming," *Sci. Rep.*, vol. 7, no. 1, Nov. 2017, Art. no. 16195.

[36] M. Janni et al., "In vivo phenotyping for the early detection of drought stress in tomato," *Plant Phenomics*, vol. 2019, 2019, Art. no. 6168209.

[37] C. Diacci et al., "Diurnal in vivo xylem sap glucose and sucrose monitoring using implantable organic electrochemical transistor sensors," *Iscience*, vol. 24, no. 1, Jan. 2021, Art. no. 101966.

[38] C. G. Bischak, L. Q. Flagg, and D. S. Ginger, "Ion exchange gels allow organic electrochemical transistor operation with hydrophobic polymers in aqueous solution," *Adv. Mater*, vol. 32, no. 32, Aug. 2020, Art. no. e2002610.

[39] K. Xie et al., "Organic electrochemical transistor arrays for real-time mapping of evoked neurotransmitter release in vivo," *Elife*, vol. 9, Feb. 2020, Art. no. e50345.

[40] R. Zhang et al., "Multi-channel AgNWs-doped interdigitated organic electrochemical transistors enable sputum-based device towards noninvasive and portable diagnosis of lung cancer," *Mater. Today Bio*, vol. 16, 2022, Art. no. 100385.

[41] W. Lee et al., "Transparent, conformable, active multielectrode array using organic electrochemical transistors," *Proc. Natl. Acad. Sci. USA*, vol. 114, no. 40, pp. 10554–10559, Oct. 2017.

[42] W. Lee et al., "Nonthrombogenic, stretchable, active multielectrode array for electroanatomical mapping," *Sci. Adv.*, vol. 4, no. 10, Oct. 2018, Art. no. eaau2426.

[43] J. Liu et al., "Fully stretchable active-matrix organic light-emitting electrochemical cell array," *Nat. Commun.*, vol. 11, no. 1, Jul. 2020, Art. no. 3362.

[44] A. E. Aliev and H. W. Shin, "Image diffusion and cross-talk in passive matrix electrochromic displays," *Displays*, vol. 23, no. 5, pp. 239–247, Nov. 2002.

[45] W. Lee and T. Someya, "Emerging trends in flexible active multielectrode arrays," *Chem. Mater.*, vol. 31, no. 17, pp. 6347–6358, Sep. 2019.

[46] D.-H. Kim et al., "Epidermal electronics," *Science*, vol. 333, no. 6044, pp. 838–843, 2011.

[47] J. Muller et al., "High-resolution CMOS MEA platform to study neurons at subcellular, cellular, and network levels," *Lab. Chip*, vol. 15, no. 13, pp. 2767–2780, Jul. 2015.

[48] P. Gkoupidenis, D. A. Koutsouras, and G. G. Malliaras, "Neuromorphic device architectures with global connectivity through electrolyte gating," *Nat. Commun.*, vol. 8, May 2017, Art. no. 15448.

[49] I. R. Minev et al., "Electronic dura mater for long-term multimodal neural interfaces," *Science*, vol. 347, no. 6218, pp. 159–163, 2015.

[50] N. Matsuhisa et al., "Printable elastic conductors with a high conductivity for electronic textile applications," *Nature Commun.*, vol. 6, no. 1, pp. 1–11, 2015.

[51] A. Williamson et al., "Localized neuron stimulation with organic electrochemical transistors on delaminating depth probes," *Adv. Mater*, vol. 27, no. 30, pp. 4405–4410, Aug. 2015.

[52] D. A. Henze, Z. Borhegyi, J. Csicsvari, A. Mamiya, K. D. Harris, and G. Buzsaki, "Intracellular features predicted by extracellular recordings in the hippocampus in vivo," *J. Neurophysiol.*, vol. 84, no. 1, pp. 390–400, Jul. 2000.

[53] P. Bartho, H. Hirase, L. Monconduit, M. Zugaro, K. D. Harris, and G. Buzsaki, "Characterization of neocortical principal cells and interneurons by network interactions and extracellular features," *J. Neurophysiol.*, vol. 92, no. 1, pp. 600–608, Jul. 2004.

[54] A. Mohanty et al., "Reconfigurable nanophotonic silicon probes for submillisecond deep-brain optical stimulation," *Nat. Biomed. Eng.*, vol. 4, no. 2, pp. 223–231, Feb. 2020.

[55] G. Lind, C. E. Linsmeier, and J. Schouenborg, "The density difference between tissue and neural probes is a key factor for glial scarring," *Sci. Rep.*, vol. 3, no. 1, pp. 1–7, Oct. 2013.

[56] S. Nahavandi et al., "Microfluidic platforms for biomarker analysis," *Lab Chip*, vol. 14, no. 9, pp. 1496–1514, 2014.

[57] G. Yang et al., "A health-IoT platform based on the integration of intelligent packaging, unobtrusive bio-sensor, and intelligent medicine box," *IEEE Trans. Ind. Inform.*, vol. 10, no. 4, pp. 2180–2191, Nov. 2014.

[58] P. Andersson Ersman et al., "All-printed large-scale integrated circuits based on organic electrochemical transistors," *Nat. Commun*, vol. 10, no. 1, Nov. 2019, Art. no. 5053.

[59] X. Ren et al., "A low-operating-power and flexible active-matrix organic-transistor temperature-sensor array," *Adv. Mater*, vol. 28, no. 24, pp. 4832–4838, Jun. 2016.

[60] J. Viventi et al., "Flexible, foldable, actively multiplexed, high-density electrode array for mapping brain activity in vivo," *Nat. Neurosci.*, vol. 14, no. 12, pp. 1599–1605, Nov. 2011.

[61] H. Fang et al., "Capacitively coupled arrays of multiplexed flexible silicon transistors for long-term cardiac electrophysiology," *Nat. Biomed. Eng.*, vol. 1, no. 3, 2017, Art. no. 0038.

[62] W. Lee et al., "Nonthrombogenic, stretchable, active multielectrode array for electroanatomical mapping," *Sci. Adv.*, vol. 4, no. 10, 2018, Art. no. eaau2426.

[63] D. W. Park et al., "Graphene-based carbon-layered electrode array technology for neural imaging and optogenetic applications," *Nat. Commun.*, vol. 5, no. 1, Oct. 2014, Art. no. 5258.

[64] G. Buzsáki, "Large-scale recording of neuronal ensembles," *Nature Neurosci.*, vol. 7, no. 5, pp. 446–451, 2004.

[65] D. Khodagholy et al., "NeuroGrid: Recording action potentials from the surface of the brain," *Nature Neurosci.*, vol. 18, no. 2, pp. 310–315, 2015.

[66] S. I. Park et al., "Soft, stretchable, fully implantable miniaturized optoelectronic systems for wireless optogenetics," *Nature Biotechnol.*, vol. 33, no. 12, pp. 1280–1286, 2015.

[67] M. Kaltenbrunner et al., "An ultra-lightweight design for imperceptible plastic electronics," *Nature*, vol. 499, no. 7459, pp. 458–463, 2013.

[68] Y. Jimbo et al., "An organic transistor matrix for multipoint intracellular action potential recording," *Proc. Natl. Acad. Sci. USA*, vol. 118, no. 39, Sep. 2021, Art. no. e2022300118.

[69] R. Giridharagopal et al., "Electrochemical strain microscopy probes morphology-induced variations in ion uptake and performance in organic electrochemical transistors," *Nat. Mater*, vol. 16, no. 7, pp. 737–742, Jul. 2017.

[70] F. Jonas and L. Schrader, "Conductive modifications of polymers with polypyrroles and polythiophenes," *Synthetic Met.*, vol. 41, no. 3, pp. 831–836, May 1991.

[71] G. Heywang and F. Jonas, *Poly (alkylenedioxythiophene) S—New, Very Stable Conducting Polymers*. Hoboken, NJ, USA: Wiley Online Library, 1992.

[72] M. Dietrich, J. Heinze, G. Heywang, and F. Jonas, "Electrochemical and spectroscopic characterization of polyalkylenedioxythiophenes," *J. Electroanalytical Chem.*, vol. 369, no. 1/2, pp. 87–92, May 1994.

[73] I. Winter, C. Reese, J. Hormes, G. Heywang, and F. Jonas, "The thermal aging of poly(3,4-ethylenedioxythiophene) - an Investigation by X-Ray-Absorption and X-Ray photoelectron-spectroscopy," *Chem. Phys.*, vol. 194, no. 1, pp. 207–213, May 1995.

[74] A. Giovannitti et al., "Redox-Stability of Alkoxy-BDT copolymers and their use for organic bioelectronic devices," *Adv. Funct. Mater.*, vol. 28, no. 17, Apr. 2018, Art. no. 1706325.

[75] A. Giovannitti et al., "Energetic control of redox-active polymers toward safe organic bioelectronic materials," *Adv. Mater*, vol. 32, no. 16, Apr. 2020, Art. no. e1908047.

[76] J. Chen et al., "Highly stretchable organic electrochemical transistors with strain-resistant performance," *Nat. Mater*, vol. 21, no. 5, pp. 564–571, May 2022.

[77] G. D. Spyropoulos, J. N. Gelinas, and D. Khodagholy, "Internal ion-gated organic electrochemical transistor: A building block for integrated bioelectronics," *Sci. Adv.*, vol. 5, no. 2, Feb. 2019, Art. no. eaau7378.

[78] M. J. Donahue et al., "High-performance vertical organic electrochemical transistors," *Adv. Mater*, vol. 30, no. 5, Feb. 2018, Art. no. 1705031.

[79] C. M. Tringides and D. J. Mooney, "Materials for implantable surface electrode arrays: Current status and future directions," *Adv. Mater*, vol. 34, no. 20, May 2022, Art. no. e2107207.

[80] A. Gholizadeh et al., "Fabrication of sensitive glutamate biosensor based on vertically aligned CNT nanoelectrode array and investigating the effect of CNTs density on the electrode performance," *Anal. Chem.*, vol. 84, no. 14, pp. 5932–5938, Jul. 2012.

[81] R. Liu et al., "High density individually addressable nanowire arrays record intracellular activity from primary rodent and human stem cell derived neurons," *Nano. Lett.*, vol. 17, no. 5, pp. 2757–2764, May 2017.

[82] Y. Liu, X. Li, J. Chen, and C. Yuan, "Micro/Nano electrode array sensors: Advances in fabrication and emerging applications in bioanalysis," *Front. Chem.*, vol. 8, 2020, Art. no. 573865.

[83] H. Shim, K. Sim, F. Ershad, S. Jang, and C. J. Yu, "Recent advances in materials and device technologies for soft active matrix electronics," *J. Mater. Chem. C*, vol. 8, no. 31, pp. 10719–10731, Aug. 2020.

[84] A. Dodabalapur, J. Laquindanum, H. E. Katz, and Z. Bao, "Complementary circuits with organic transistors," *Appl. Phys. Lett.*, vol. 69, no. 27, pp. 4227–4229, Dec. 1996.

[85] K. J. Baeg, M. Caironi, and Y. Y. Noh, "Toward printed integrated circuits based on unipolar or ambipolar polymer semiconductors," *Adv. Mater*, vol. 25, no. 31, pp. 4210–4244, Aug. 2013.

[86] H. D. Sun, J. Gerasimov, M. Berggren, and S. Fabiano, "n-Type organic electrochemical transistors: Materials and challenges," *J. Mater. Chem. C*, vol. 6, no. 44, pp. 11778–11784, Nov. 2018.

[87] H. Sun et al., "Complementary logic circuits based on high-performance n-Type organic electrochemical transistors," *Adv. Mater*, vol. 30, no. 9, Mar. 2018, Art. no. 1704916.

[88] P. Romele et al., "Multiscale real time and high sensitivity ion detection with complementary organic electrochemical transistors amplifier," *Nat. Commun.*, vol. 11, no. 1, Jul. 2020, Art. no. 3743.

[89] E. Stein et al., "Ambipolar blend-based organic electrochemical transistors and inverters," *Nature Commun.*, vol. 13, no. 1, pp. 1–10, 2022.

[90] A. Onwubiko et al., "Fused electron deficient semiconducting polymers for air stable electron transport," *Nat Commun*, vol. 9, no. 1, Jan. 2018, Art. no. 416.

[91] S. H. Wang et al., "Experimental evidence that short-range intermolecular aggregation is sufficient for efficient charge transport in conjugated polymers," *Proc. Nat. Acad. Sci. United States Amer.*, vol. 112, no. 34, pp. 10599–10604, Aug. 2015.